Cranfield University
School of Agriculture, Food and Environment at Silsoe

MSc
Academic year 2000-01

Eric Bappel

Investigation of topographic influences on Compact Airborne Spectrographic Imager data

Supervisor: Christophe Sannier

August 2001

This thesis is submitted in partial fulfilment of the requirements for the Degree of Master of Science in Geographical Information Management

Abstract

The 'topographic effect' is the distortion in measured radiance caused by differential illumination and viewing angles in undulating terrain. This effect is quantified for CASI imagery of the Reunion Island (French overseas territory, Indian Ocean), in an area dominated by sugar cane cover.

High-resolution digital elevation models provide a means to correct the data in a remotely sensed image for the topographic effect. By calculating the slope and aspect of a surface, the sun/surface/sensor orientation can be determined, and its effects included in a standard data processing procedure. Several algorithms of topographic correction using DEMs have been proposed, but none have gained widespread use in the remote sensing community. The goals of our research are to test two methods of topographic correction on a sugar cane stand in Reunion Island, and demonstrate if these methods should be considered before creating any vegetation map using remotely sensed data.

A digital elevation model is generated by stereoscopic analysis of aerial photography. The slope and aspect images of the study area are produced. There are the main input for the normalisation models.

The Lambertian and non-Lambertian normalisation model were found to apply over correction. Using the regression coefficients obtained for the non-Lambertian model, the Lambertian assumption can be rejected.

The results shown that it is not necessary to include a topographic correction step in the vegetation mapping process of the CASI images. This result could not be generalised to whole Reunion Island but only on area with the same topographic characteristics.

Acknowledgements

Many thanks to Christophe Sannier, and Graham Thomas at Silsoe College, for their invaluable technical advice, and for making it possible for me to complete this thesis whilst working full-time.

Thanks also to Cirad-AMIS for the use of the CASI image, computing and printing resources, which allowed me to complete this thesis. Thanks also to Benoit Caumont, Cirad technician in the Reunion Island for the field measurements, GPS points acquisition.

A special thank-you to Marc Despinoy my local supervisor for his helpful technical advice reviews.

Table of Contents

List of figures

List of tables

List of appendices

1.0 Introduction

Topographic effects on the satellite images have already been subject of a lot of research and is well known. Their influence on airborne multispectral images, as the CASI images, are less known. The objectives of this study is to quantify the influence of the topography on the CASI images covered with sugar cane.

Within studying the use of the CASI to make precision farming on some sugar cane in the reunion island, it is important to study the effects of hillsides. Indeed, the relief of the Reunion island impose fragmented location of fields, one distributed as well on flat grounds as on grounds with strong slope. So it is interesting to know if a step of radiometric normalisation of the images will be necessary.

The aims of this study can be resumed in two points :

- To correct the CASI images and determine which is the most successful model in the case of image with very high spatial (2m) and spectral (4 bands) resolutions

- To estimate the impact of the topographic effects on the pixel DN value of CASI images and the need of correction.

1.1 The topographic effect and its influence on the radiometric response

Typically processing of satellite or airborne images assume a flat representation of a part of the ground. In the field of the visible and the near infrared, these data represent the magnitude of the solar spectral irradiance reflected by the earth's surface. As such, they contain information about the state of this surface.

However, these data are considerably influenced by the topography of the studied areas. This influence can generate very different data on surfaces of the same spectral or very similar nature. It is an important problem in remote sensing notably for classifications. Indeed the algorithm of classification can assign two pixels to two different classes while they represent the same entity to the ground.

To make the radiometric correction of the images, it is necessary to associate to every pixel one or several topographic factors used by the selected topographic normalisation model. These factors allow the calculation of the parameters necessary for the models, notably the sun angle of incidence and the exitance angle. To make these calculations, digital elevation model of the study area is necessary.

Two methods were used to obtain the required digital model : the use of a GPS in static mode on the study area and the semiautomatic method using a stereoscopic analysis of aerial photography. The topographic factors necessary are the slope and the aspect.

1.2 Methods of correction of the topographic effect

The fast progress in the creation of a DEM is susceptible to bring a considerable help for the topographic correction. There is at present not enough satisfactory model of correction in the literature. Among the topographic effects, the only one generally taken into account for the radiometric correction is sun incidence angle effect. Some models of correction consider more effects coming from diffuse illumination and shadow.

High-resolution digital elevation models provide a means to correct the data in a satellite image for the topographic effect. By calculating the slope and aspect of a surface, the sun/surface/sensor orientation can be determined, and its effects included in a standard data processing procedure. Several algorithms of topographic correction using DEMs have been proposed, but none have gained widespread use in the remote sensing community (Reeder, 1999).

The use of ration algorithms has been reported to partly resolve the problem of variable illumination, provided that the atmospheric path radiance term is eliminated (Kowalik et al., 1983; Chavez and Mitchell, 1977; Rowan et al., 1977). This imply that an empirical correction based on digital slope/aspect data would be more appropriate than a ratio correction.

1.2.1 Lambertian normalisation model

As shown in figure 1.1, the methods of correction are based on the geometry between the sun, the local surface plane and the sensor.

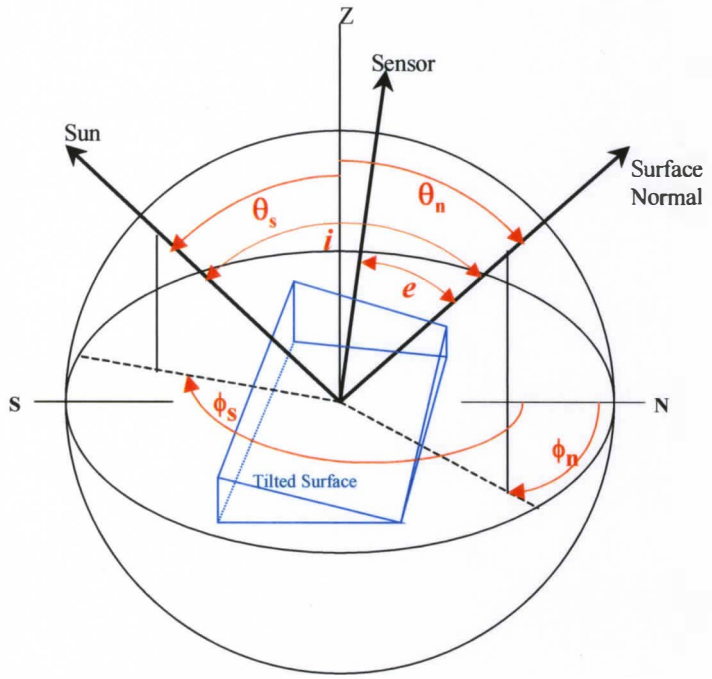

Figure 1.1, Sun-surface-sensor geometry

With :

i = solar incidence angle
e = exitance angle
θ_s = solar zenith angle
θ_n = surface normal zenith (slope)
ϕ_s = solar azimuth angle
ϕ_n = surface aspect of the slope angle

A Lambertian surface is presumed to be a perfect diffuse reflector, appearing equally bright from all viewing directions. Therefore, a Lambertian correction function attempts to correct only for differences in illumination caused by the orientation of the surface (Jones et al., 1988). Radiance is assumed to be proportional to the cosine of the incidence angle. The solar incidence angle (i) is the angle between the surface normal and the solar beam, and may be calculated by (Smith et al., 1980; Holben and Justice, 1980) :

$$\cos i = \cos \theta_n \cos \theta_s + \sin \theta_n \sin \theta_s \cos (\phi_s - \phi_n) \qquad \textbf{(1)}$$

Northern slopes approaching the point where the surface is in shadow ($\cos i < 0$) should, according to the Lambertian assumption, have no reflectance. However, during day time, diffuse sky irradiance will always reach the surface, and part of it will be reflected.

It may be advocated that the surface itself may still be nearly Lambertian but, as seen from the platform, it is not. Several authors have found that the sky irradiation cannot be neglected for pixels with low direct illumination (e.g., Proy et al., 1989; Kimes and Kirchner, 1981), and the non-Lambertian assumption gives superior results for vegetated surfaces (Colby, 1991; Jones et al., 1988; Leprieur et al., 1988; Thomson and Jones, 1990). If atmospheric path radiance is removed in advance and sky irradiance is neglected, the Lambertian assumption cosine correction is (Smith et al., 1980) :

$$L_n(\lambda) = \frac{L(\lambda)}{\cos i} \qquad W.m^{-2}.sr^{-1} \qquad \textbf{(2)}$$

where : $L_n(\lambda)$ is the effective normal response that would be measured when the incidence and slope angles both are at zero, i.e., when the surface is perpendicular to a sun in zenith.

When the sun is not in zenith, correction of the radiance of an inclined surface to the radiance of the projected horizontal surface would be achieved by the function (Teillet et al., 1982) :

$$L_H(\lambda) = L_T(\lambda)\frac{\cos\theta_S}{\cos i} \qquad W.m^{-2}.sr^{-1} \qquad \textbf{(3)}$$

Where : $L_H(\lambda)$ is the radiance for a horizontal surface
$L_T(\lambda)$ is the radiance observed over the inclined terrain.

Note that the Lambertian model does not take account of the exitance angle, angle between the sensor and the normal to the surface.

The Lambertian normalisation model is simple to apply but presume a Lambertian surface. The majority of previous works have shown that this correction is inappropriate for forest vegetation, with an exception of high solar elevation.
The model generally causes over-correction of northern slopes. The most common way to account for the non-Lambertian behaviour of vegetation has been to employ the Minnaert constant (Colby, 1991; Jones et al., 1988).

From equation (3) a model could be build to transform the Digital Number (radiance or reflectance) of a raw image to a normalised image thanks to image processing software such as Erdas Imagine.

1.2.2 Non-Lambertian normalisation model

This function was originally proposed for lunar application by Minnaert (1941), in which the constant k was used to describe the surface roughness. In the study by Smith et al. (1980), the function was used to give satellite radiance by

$$L(\lambda,\theta_n) = L_n(\lambda)\cos^{k(\lambda)} i \cos^{k(\lambda)-1}\theta_n \qquad W.m^{-2}.sr^{-1} \qquad \textbf{(4)}$$

Where k is the Minnaert constant. The constant can be derived by first linearizing equation (4). Then obtaining the regression value for k, using (Smith et al., 1980; Colby, 1991),

$$L\cos\theta_n = L_n \cos^k i \cos^k \theta_n$$

and

$$\log(L\cos\theta_n) = \log L_n + k\log(\cos i \cos\theta_n)$$

where $y = \log(L \cos\theta_n)$, the response variable;
$x = \log(\cos i \cos\theta_n)$, the independent variable; and
$b = \log(L_n)$

The linear form is obtained from $y = kx + b$. The equation is then solved for k, which represents the Minnaert constant.

Low value of k imply asymmetrical diffuse scattering and a value equal to 1 defines symmetrical diffuse scattering, a Lambertian surface.

Note that for $k = 1$ equation (4) is reduce to equation (3). Most of the "Minnaert papers" showed that k value, or the degree of non-Lambertian behaviour, is wavelength dependant and, consequently, presented one value for each spectral band.

k is scene dependent because, varies in relationship with the cover type, wavelength and solar elevation angle. So k have to be determine from each scene to normalise, from each cover type on the same scene. This is the limitation of the non-Lambertian model because derivation of k value is complex and takes time in term of calculation.

2.0 Presentation of the study area and data available

The **ICARE** (**I**nterorganism **C**ASI **R**éunion **E**xperimentation) project, was realised in May, 1996 on the Reunion Island. The objectives of the program ICARE were to use the CASI system (Compact Airborne Spectrographic Imager) to acquire images allowing to answer to the specific demands of the various organisations. The CASI system was able to be used has Reunion thanks to Borstad come from Canada. It was installed on a plane (for the production of the vertical view angle) and on a helicopter (allowing horizontal or oblique angle).

2.1 Presentation of the study area

Located in the Indian Ocean, at 800 km east of Madagascar (figure 2.1), the Reunion island constitutes with Mauritius and Rodrigue, the archipelago of Mascareignes. Its environment (rain forest, its volcanic massifs and its plantations of sugar cane) makes it a colourful island. The area of the Reunion Island is about 2500 Km^2. Sugar cane crop represents 30 000ha.

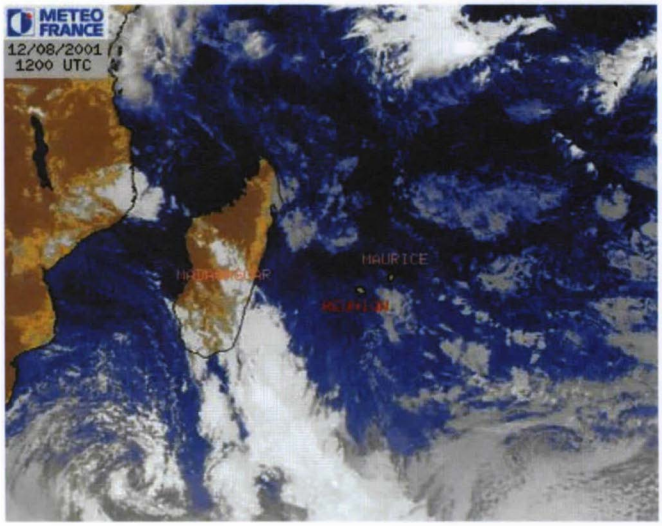

Figure 2.1, location of the Reunion Island in the Indian Ocean, Meteosat image, Meteo France.

The study area is situated in the north east part of the island, (figure 2.2). The location of the study area was selected where CASI images and agronomic data of May 15th 1996 were available.

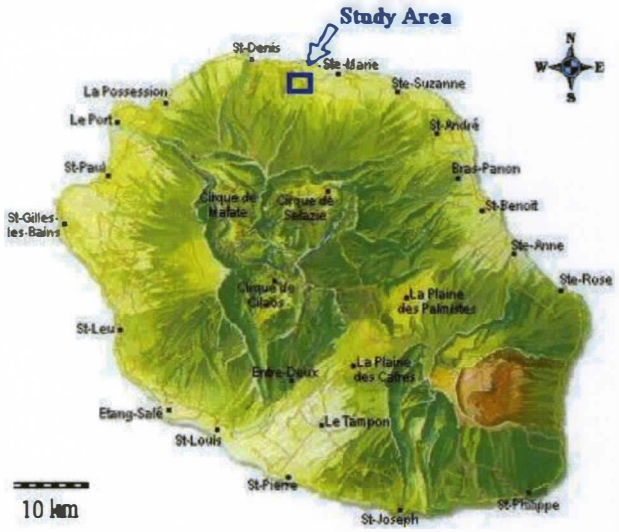

Figure 2.2, location of the study area on the Reunion Island.

Therefore the surface of the study area was decreased to 2.34 km2. The figure 2.3 shows the location of the area on a IGN (Institut de Géographie National) topographic map at 1: 25 000 scale as well as the geographic coordinates in UTM WGS 84 zones 40s of the corners. The main land use in this area is sugar cane crop.

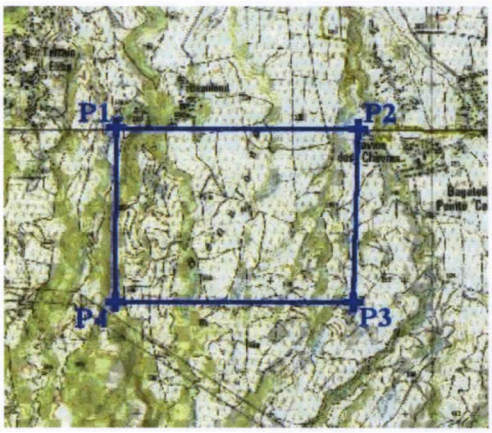

Figure 2.3, location of the study area on IGN topographic map.

Coordinates of the corner points in UTM WGS 84 zones 40s:

Points	East (m)	North (m)
P1	350 700	7 686 390
P2	352 010	7 686 430
P3	352 050	7 685 350
P4	350 880	7 685 260

The elevation range of the area is 178 to 361 metres above the sea level. The slope angle range is between 0° to 60° with a mean value of 7.3°, calculated from the topographic map. The dominant aspect is north facing due to the location, on the hillside of the old volcano, *le Piton des neiges.*

2.2 *Description of the datasets*

2.2.1 CASI data

During the data acquisition campaign ICARE, a CASI image with 4 spectral bands and a spatial resolution of 2m was recorded on May 15th, 1996.

The technical characteristics of the CASI image *May15_211.img* are:

- Spatial Resolution : 2m
- Spectral Resolution : 4 channels

1. :426.0 – 459.2 nm
2. :531.2 – 547.1 nm
3. :628.7 – 637.6 nm
4. :737.8 – 744.9 nm

- Radiometric Resolution : 16bits
- Date and time of acquisition : May 15th, 1996 at 11.00 am (local time)
- Solar elevation : 47.38°
- Solar azimuth : 27.96°

Note that the solar elevation and azimuth were obtained using the Solar Position Calculator of the NOAA Surface Radiation Research Branch.

Further technical characteristics of the CASI sensor are given in appendix 1.

The raw data are images with 1150m width and a length of 7800m. A true color composite and a false color composite are shown in the figure 2.4 and a map is available in appendix 1a.

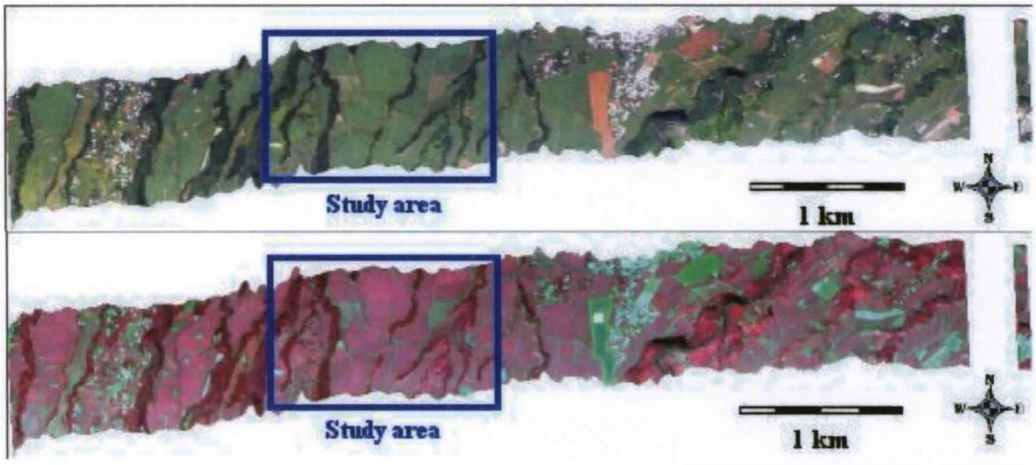

Figure 2.4, up image true colour composite raw reflectance CASI image and below a false color composite.

The radiometric correction, DN to reflectance, was performed by Borstad Cie. The geometric correction of the subset was performed with a RMS Error of 4.3 using 35 GCP points. The RMS Error value could not be decreased.

This comes from the fact that the image was recorded from an aerial platform and a lot of distortion occurred, due to the movement of the plane. The 35 GCP points were collected on the field with a GPS Trimble pro XRS in differential mode. The differential signal for the correction comes from the Omnistar satellite. The satellite creates a virtual base around the location of acquisition that allows a differential correction in real time. The mean RMS Error of the 35 GCP point (in x and y) is about 0.3 m. The figure below (figure 2.5) shows a subset of the raw image that containing the study area and the location of the 35 GCP points used for the geometric correction. The image was resampled using the nearest neighbour algorithm to preserve the original pixel brightness value with a 3 degree polynomial function.

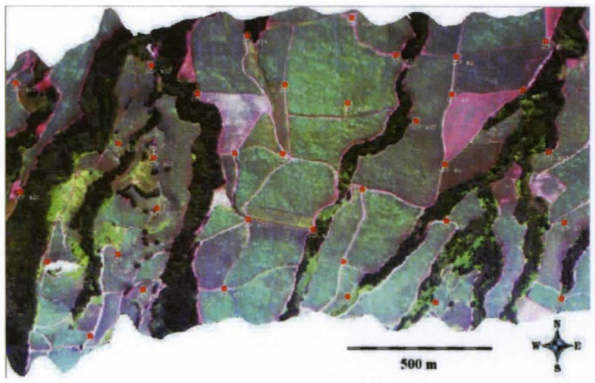

Figure 2.5, subset of the study area and location of the 35 GCP

2.2.2 Digital Elevation Model

The digital elevation model was supposed to be generated using a GPS Trimble pro XRS in static mode. The points had to be recorded using differential correction to ensure a low RMS Error, in relation with the size of the image pixels, 2 meters. But it was not possible to obtain the DEM by this method, no technician was available at the proper time. So we have to use another method to derive the DEM, which is the stereoscopic analysis of aerial photography. This method required a specific software package : Photomod (version 1.51 developed by C.H.S., Paris)

Photomod (version 1.51) is a software of digital photogrammetry mainly intended for relief observation, measures in 3D, creation of digital elevation models (DEM) of ground or objects, ortho-images and profiles, lines of contour level and 3D objects. The input data to the system are digital stereoscopic images in the form of files, obtained either directly from numeric device , or scanned.

A stereoscopic images couple is a couple of photographic images of the same sites or the same object, takes from two different positions, on which is based the calculation of the spatial model (3D) which consists in throwing the points of both images in a space 3D.

This projection is defined by some parameters fixed or calculated by the procedures of internal, relative and absolute orientation.

To calculate absolute orientation, it is necessary to have a minimum of reference data, recognisable points on the images with known coordinates, GPS points for example.

It was possible to obtain 15 GPS points with low RMSE for the absolute orientation. The table 2.1 gives the coordinates of the 15 points in Long/Lat WGS 84 and the elevation with the RMSE in meter archived for each points.

Points	Longitude	Latitude	RMSE (m)	Elevation	RMSE (m)
1	55,6088772	-20,9347268	0,374	180,250	0,98
2	55,6058125	-20,9324029	0,355	174,921	1,007
3	55,5985153	-20,9269846	0,258	150,889	0,789
4	55,5965327	-20,9302963	0,18	185,389	0,612
5	55,5897227	-20,9282681	0,496	204,818	1,566
6	55,5827691	-20,9372283	0,234	303,101	0,465
7	55,5748668	-20,9338953	0,518	289,017	1,032
8	55,5674713	-20,9305283	0,227	253,64	0,597
9	55,5651427	-20,9370967	0,282	336,101	0,552
10	55,5606611	-20,9378656	0,393	360,079	0,783
11	55,5620747	-20,9292895	0,35	260,948	0,87
12	55,5557889	-20,9343241	0,247	303.853	0,838
13	55,5503732	-20,9367501	0,309	356,14	0,76
14	55,5380725	-20,9379248	0,315	379,902	0,616
15	55,5498933	-20,9282003	0,728	254,033	1,031

Table 2.1, GPS points coordinates

The location of each points is available in appendix 2.
The data used for the generation of the DEM was the contour line (every 10 meter) digitalised from the digital topographic data base of the IGN and points added manually using the 3D visualisation of Photomod. This method was time consuming but it was the only issue to generate the DEM of the area in order to obtain the topographic parameters (slope and aspect) required for the application of the topographic model. Information about the DEM are shown in the table 2.2.

Number of point	**6619**
Number of side	**19824**
Number of triangle	**13206**

Table 2.2, DEM's characteristics

In order to test the accuracy of the DEM (x, y and z), elevation value and coordinates of the 15 GPS points was recorded on the DEM. An RMS Error of 1.5m was found for the x and y coordinates and a value of 3.2m for the elevation accuracy.

The data generated by Photomod were exported in .dxf format, it's a Triangulated Irregular Network, an image of the TIN is available on appendix 3a. With Photomod, it's possible to obtain an overlap of the aerial photography on the DEM, figure 2.6.

Figure 2.6, overlap of the aerial photography on the DEM

An elevation raster was generated using the import option of Erdas Imagine, figure 2.7. The black color correspond to the lowest elevation and the white color to the highest.

Figure 2.7, raster elevation of the DEM

2.2.3 Extraction of the topographic characteristics

The topographic analysis tools of Erdas Image were used to generate slope and aspect raster images from the elevation data (figures 2.8 and 2.9). The method used by Erdas Imagine for calculating the slope and aspect data are described in appendix 3.

Figure 2.8, slope raster

Figure 2.9, aspect raster

The slope image (in degree) is coded by 0, black color is due to a slope of 0° degree and 90, the white color, due to a slope of 90°. The lowest slope is 0°, the highest is 86° with a mean of 10.7°.

For the slope raster, a DN value of 0 is due to north with degrees increasing clockwise. 90 due to east 180 south 270 west.

From the slope and aspect raster, it is possible to generate images of cos(i)and cos(e), which are the 2 main inputs into the normalisation models (figures 2.10 and 2.11). The methods used to produce both the cos(i) and cos(e) images are also described in the appendix 3.

Figure 2.10, cos(i) image

Figure 2. 11, cos(e) image

2.2.4 Land use database

The land use data available on the study area give information about the variety of the sugar cane present in the area, the planting date, the stage of the crop and the date of harvesting in 1995 and 1996. It is important to have this information in order to locate homogenous areas, with the same variety of sugar cane at the same stage. The data are a geographical information layer, geographically referenced. The fields were represented by polygons. A layout of the study area is available on appendix 4, the layer of information was overlapped on the aerial ortho-photography of the study area. The table in appendix 4 summarises the data.

3.0 Selection and application of topographic normalisation models

3.1 Selection of the topographic normalisation models

In order to evaluate the efficiency of the topographic normalisation models, two models have been selected :

- The Lambertian model
- The non-Lambertian model

The Lambertian model has been selected because it is the simplest topographic normalisation model and it could be sufficient if the surface could be considered as a Lambertian surface, that is to say a perfect reflector. The model requires a DEM of the area, the solar azimuth and zenithal angles.

The non-Lambertian model was selected as it gave good results in previous studies, see section 1.2.2.. All the necessary parameters could be derived from the data available in this study.

3.2 Application of the Lambertian Model

The Lambertian assumption cosine correction is described by the equation (2), see section 1.2.1.

$$\mathrm{Ln}(\lambda) = \frac{\mathrm{L}(\lambda)}{\cos \mathrm{i}}$$

The application of the Lambertian model is available within the Erdas Imagine processing tools. The raw and corrected image by the Lambertian model is shown in figure 3.1 and 3.2. Both are geometrically corrected.

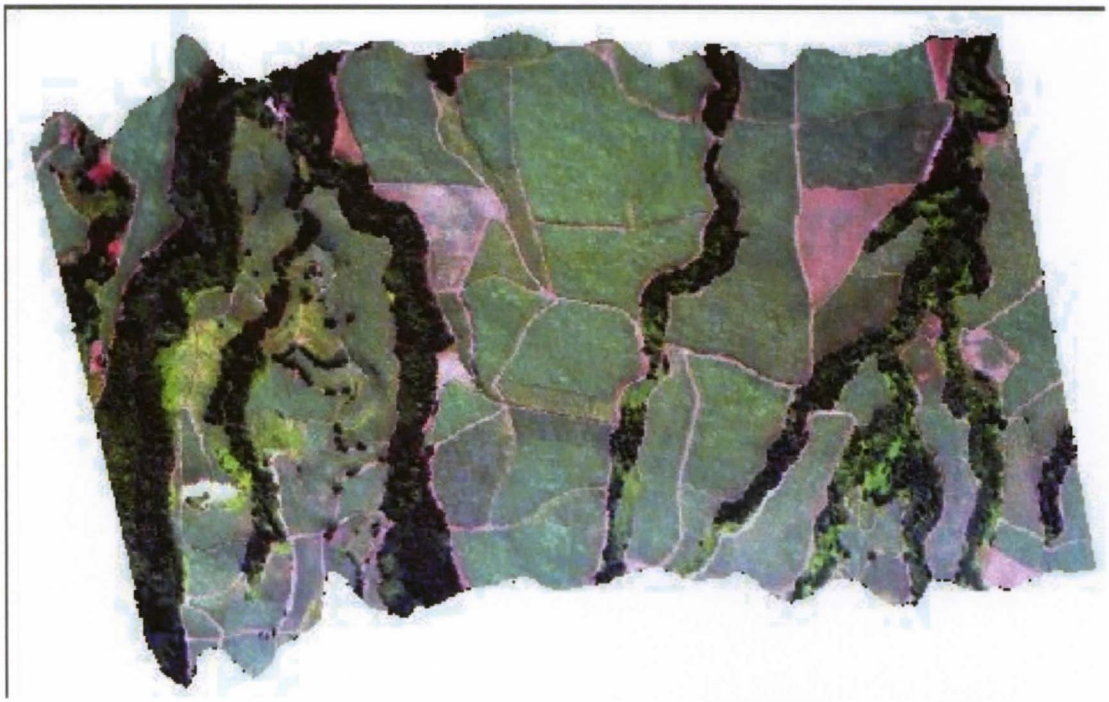

Figure 3.1, raw CASI image in true color composite

Figure 3.2, corrected CASI image by the Lambertian model, true color composite

Note that the two lines at the left and right part of the image come from the process of the correction. It is the limit of the DEM, shorter than the CASI image. Analysis and discution of the result will be done in the section 4.0.

3.3 Application of the non-Lambertian model

As we expressed in the section 1.2.2, the Minnaert constant k, wavelength dependant, have to be derived empirically from the image. This provides the means to test the Lambertian assumption on the study area. The range of k is between 0 and 1. If k = 1, the surface could be considered to be Lambertian. Values of k not equal to 1 imply a combination of diffuse and specular scattering.

So the lambertian model can be build using the equation below :

$$\log(L\cos\theta_n) = \log Ln + k\log(\cos i\cos\theta_n)$$

where $y = \log(L\cos\theta_n)$, the response variable;
$x = \log(\cos i\cos\theta_n)$, the independent variable; and
$b = \log(Ln)$

The linear form is obtained from $y = kx + b$. The equation is then solved for k, the Minnaert constant.

Note that for the case of the CASI sensor, the angle between the sensor and the surface normal is equal to zero for all pixels in the image, correction done by Borstad. So, in this study, the surface normal angle (θ_n) is equal to the exitance angle (e) to avoid any confusion.

The Minnaert constant, wavelength dependant, have to be determined for each band using a pixels sample from the CASI image. The method consists in making an extraction of the DN value for observed reflectance in each band and the corresponding value of cos(i) and cos(e), and find the k value, for each band, by linear regression of the equation described above.

According to Holmes (1998), the pixels sample for regression has to be chosen in an area with slope value of at least 15°. The sample used for regression was obtained using 26 pixels. The regression results for each CASI band are given in the table 3.1.

CASI band	K-values	R^2-values
1	0.19	0.61
2	0.24	0.65
3	0.38	0.71
4	0.42	0.70

Table 3.1, Results of Minnaert constant regression.

The k-values in the table above were accepted as Minnaert constants for sugar cane cover for each CASI band. Note that the value of k increases with the wavelength of the CASI band, which is in the line with the finding of Colby (1991) with SPOT data. When the value of k increases, the surface behaves in a more and more Lambertian manner.

The application of the non-Lambertian model was performed in the "Spatial Modeller", Erdas Imagine software, using for each band :

$$L_{n\ (Band1)} = (L_{obs} \cdot \cos(\theta_n)) / (\cos^{0.19}(i) \cdot \cos^{0.19}(\theta_n))$$

$$L_{n\ (Band2)} = (L_{obs} \cdot \cos(\theta_n)) / (\cos^{0.24}(i) \cdot \cos^{0.24}(\theta_n))$$

$$L_{n\ (Band3)} = (L_{obs} \cdot \cos(\theta_n)) / (\cos^{0.38}(i) \cdot \cos^{0.38}(\theta_n))$$

$$L_{n\ (Band4)} = (L_{obs} \cdot \cos(\theta_n)) / (\cos^{0.42}(i) \cdot \cos^{0.42}(\theta_n))$$

The corrected image by the non-Lambertian model is shown in the figure 3.3

Figure 3.3, Image in true color composite corrected by the non-Lambertian model

The Lambertian and non-Lambertian normalisation models were applied to the corrected CASI image. Note that the determination of the Minnaert constant for each band is time consuming and it was not possible to increase the coefficient of correlation.

4.0 Validation and measures of model performance

The diminution of the topographic effect on the corrected images will be done using relative analysis, comparison between the raw and corrected image.

The performance of the models is assessed using 3 indicators :

- Visual analysis
- Statistical analysis
- Improvement of the classification accuracy

4.1 Visual analysis

If it is possible to have a sensitive perception of the forms of the relief on a raw image, it can be considered that there are topographic effects. Corrected image should then show an enfeeblement of this perception and the more the model is correct the more the corrected image should then show an enfeeblement of this perception (Yang, 1990). So a first evaluation of the performance of the model can be performed by this criterion.

Thanks to the DEM and CASI overlapped image, it was possible to locate an area where the perception of the form of the relief existed. The figure 4.1 shown this location.

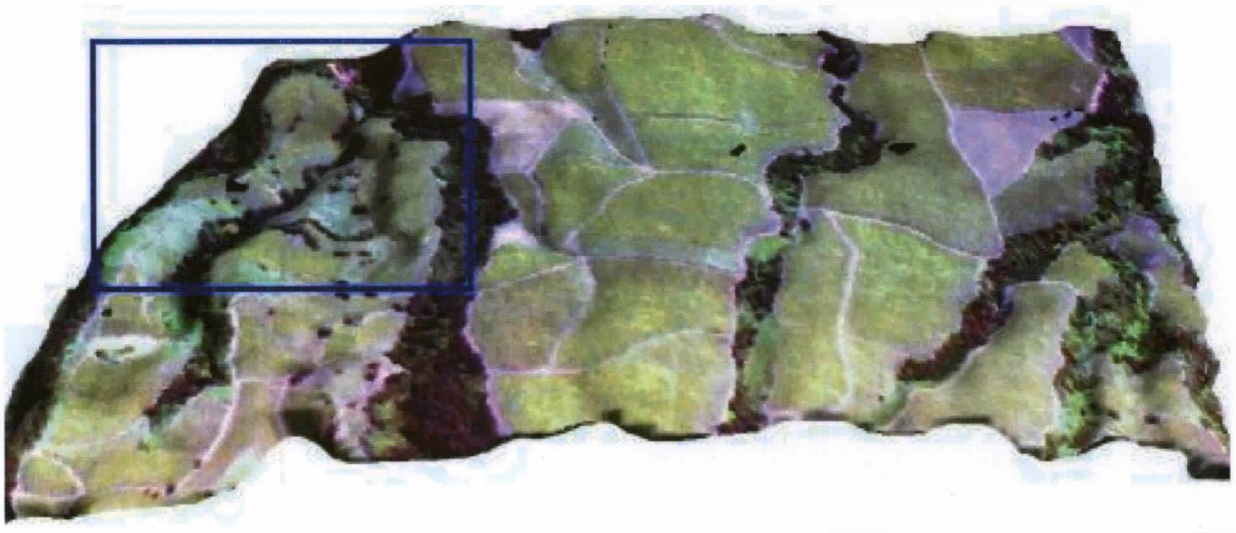

Figure 4. 1, CASI image draped on the DEM, the blue rectangle is the area of interest for the visual analysis

A subset of this area has been produced for each corrected image in order to compare and evaluate the performance of each model on this criterion, perception of relief. The figure 4.2 bellow represents the three subsets.

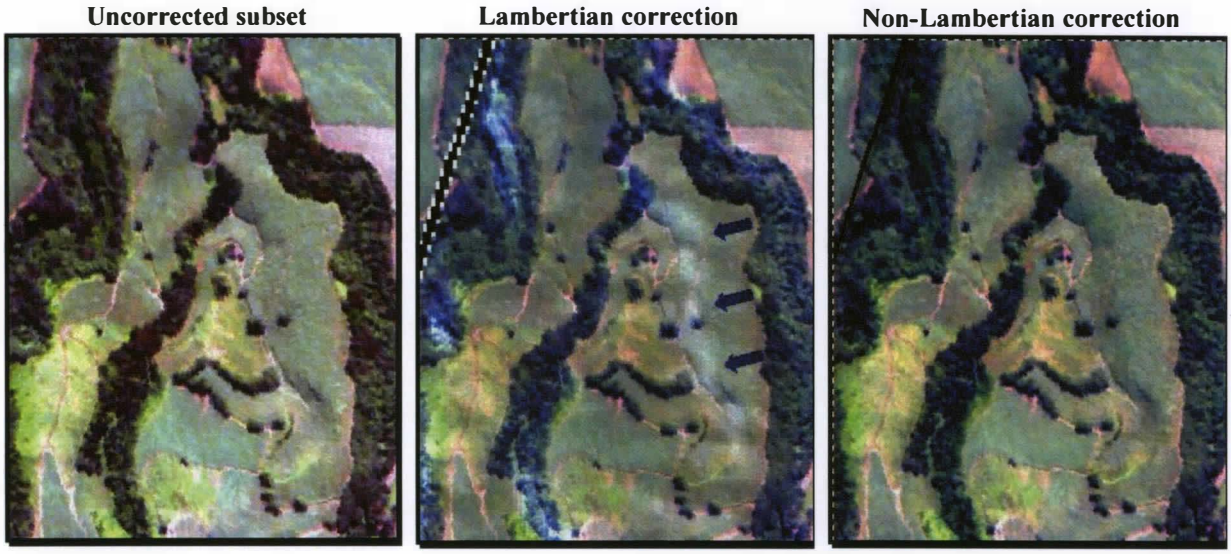

Figure 4.2, the three subset chosen for the visual analysis

The perception of the relief is present on the uncorrected image. The Lambertian model applies an over correction, enlightenment focused by the blue arrows. In the Lambertian correction the perception of the relief seems to have decreased. The over correction applied by the Lambertian model is not present on the image corrected by the non-Lambertian model. The perception of the relief is more or less the same. The correction applied by the non-Lambertian model seems to have an homogenous influence on the area, did not take in account the relief. On the criterion of the diminution of the relief perception, the Lambertian correction is more accurate than the non-Lambertian model, but the problem of over correction is still present. The Lambertian model identifies the area where the radiometric correction has to be applied to decrease the perception of the relief. But the correction is not adequate.

4.2 Statistical analysis

The model of correction seems to be accurate if the standard deviation of the pixels brightness value in an homogenous area is decreased by the model. In the literature, some authors make the validation of the model using the difference of the standard deviation of an homogeneous area before and after the topographic normalisation. If the model is accurate, on this criterion, the difference of the standard deviation, before and after normalisation, have to decrease. So the standard deviation of the normalised image has to be lower than in the raw image, for an homogenous cover. But a topographic normalisation could also decrease the DN value in the same time than the standard deviation. So a diminution in the standard deviation value is not in relation with the diminution of the topographic effects. Analysis of only the standard deviation is not a good indicator to measure the performance of the model. On the other hand, the performance of the model could be measured by analysis of the variation coefficient, standard deviation divided by the mean.

The analysis has been done using a pixel sample of 840 pixels, extracted from an homogenous area of sugar cane, same variety and stage.

The table 4.1 represent the result of the mean, standard deviation and variation coefficient.

		Raw value	Lambertian correction	Non-Lambertian correction
Mean	Band 1	20.43	25.66	21.35
	Band 2	25.17	31.59	26.73
	Band 3	14.25	17.95	15.59
	Band 4	106.76	133.95	123.60
Standard deviation	Band 1	1.41	1.79	1.48
	Band 2	0.87	1.21	1.15
	Band 3	0.75	1.06	1.09
	Band 4	3.09	4.41	3.82
Variation coefficient	Band 1	6.89%	6.98%	6.94%
	Band 2	3.46%	3.84%	4.30%
	Band 3	5.25%	5.93%	6.96%
	Band 4	2.90%	3.29%	3.09%

Table 4.1. results of the statistical analysis applied on homogenous area of 840 pixels.

The analysis has been done on the DN value of the image, coded in 8 bits.

Analysis of these results shows two facts :

- An increase of the mean value is done by the two models, the over correction present in the figure 4.2 is confirmed by obtaining higher mean value for the Lambertian correction than for the non-Lambertian correction. The mean value is increased by 25% for the band1, band3 and band4 and by 28% for the band 2 in the Lambertian correction. Both Lambertian and non-Lambertian model increase the mean value but the non-Lambertian model increases this value in a lower range, the over correction effect is less significant. The non-Lambertian model increases the mean DN value by a range between 4.5% for the band1 to 15.7% for the band4.

- An increase of the variation coefficient for each model in each band. The result expected was supposed to be a diminution of the variation coefficient, but an increase of the variation coefficient indicates that the model increases both the mean and the standard deviation DN value of an homogenous subset. The effect of the topographic normalisation, in this study, seems to have the opposite influence than the expected one.

Both Lambertian and non-lambertian model applied an over correction. This result could be explained by a low topographic influence on the study area on the pixels DN value.

4.3 Analysis of the improvement of the classification accuracy by the two models

It is possible to measure the performance of the model by analysis the improvement of the classification accuracy. This method was applied using a subset of the study area. The classification is based on four classes, present in the CASI image subset : two varieties of sugar cane, forest and bare soil.

The figure 4.3 shows the location where the classification has been done.

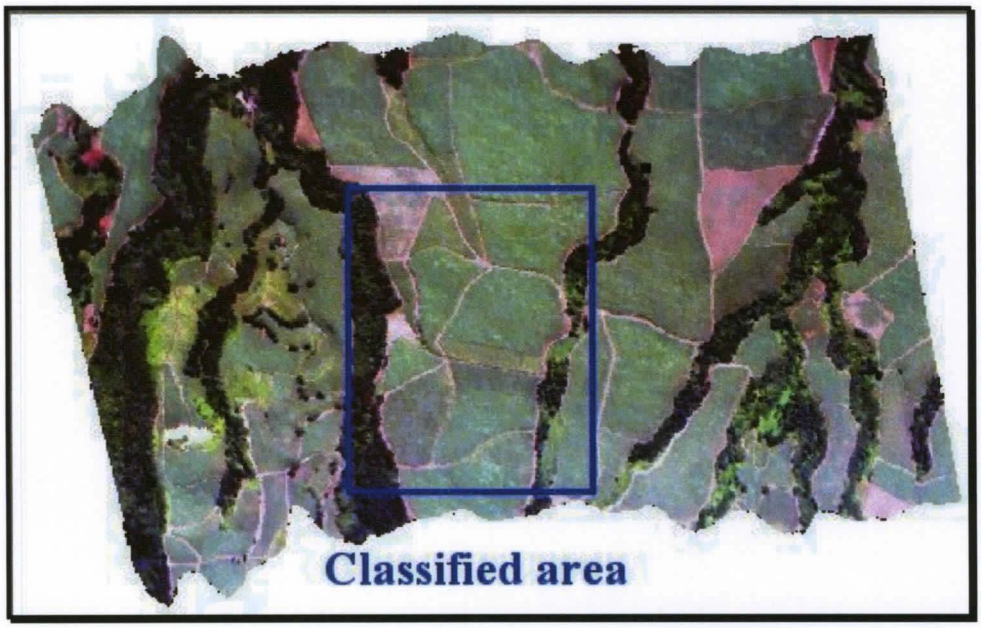

Figure 4.3, location of the classified area

The classification was performed using Erdas Image software. It is a supervised classification with nearest neighbour algorithm. The accuracy total matrix was produced in order to evaluate the performance of the model. The indicator chosen for the evaluation of the model performance in the improvement of the classification accuracy is the Overall Kappa Statistics.

The tables below resume the result of the three classifications performed on the CASI image before normalisation and after normalisation with both models.

The way to evaluate the improvement in the accuracy of the classifier is to compare the value of the Overall Kappa Statistics. It is possible to evaluate the performance of the classifier for each class using conditional Kappa for each category.

- Accuracy total matrix for the classification before normalisation :

Class Name	Reference Totals	Classified Totals	Number Correct	Producers Accuracy	Users Accuracy
forest	6	7	6	100.00%	85.71%
cane1	4	7	4	100.00%	57.14%
cane2	23	20	20	86.96%	100.00%
bare soil	7	6	6	85.71%	100.00%
Totals	40	40	36		

Overall Classification Accuracy = 90%
Overall Kappa Statistics = 0.8444

- Accuracy total matrix for the classification after normalisation by the Lambertian model :

Class Name	Reference Totals	Classified Totals	Number Correct	Producers Accuracy	Users Accuracy
forest	6	6	4	66.67%	66.67%
cane1	15	18	11	73.33%	61.11%
cane2	12	9	5	41.67%	55.56%
bare soil	7	7	6	85.71%	85.71%
Totals	40	40	26		

Overall Classification Accuracy = 65%
Overall Kappa Statistics = 0.5075

- Accuracy total matrix for the classification after normalisation by the non-Lambertian model :

Class Name	Reference Totals	Classified Totals	Number Correct	Producers Accuracy	Users Accuracy
Forest	5	4	4	80.00%	100.00%
bare soil	7	7	6	85.71%	85.71%
cane2	25	18	18	72.00%	100.00%
cane1	3	11	2	66.67%	18.18%
Totals	40	40	30		

Overall Classification Accuracy = 75%
Overall Kappa Statistics = 0.6183

The accuracy total matrices were generated using 40 ground control points. The detailed results of the three classifications are available on appendix 5.

The result of the classification before and after normalisation by the Lambertian and non-Lambertian models shows that the higher accuracy is obtained in the classification of the raw, before normalisation. The non-Lambertian model decreases the accuracy of the classification by 16.7 % and the Lambertian model by 27.8%. The diminution of the classification accuracy by the two models represents an increase of the misclassified pixels.

The figure 4.4 representing the raster classified images and the table 4.2 indicates the legend.

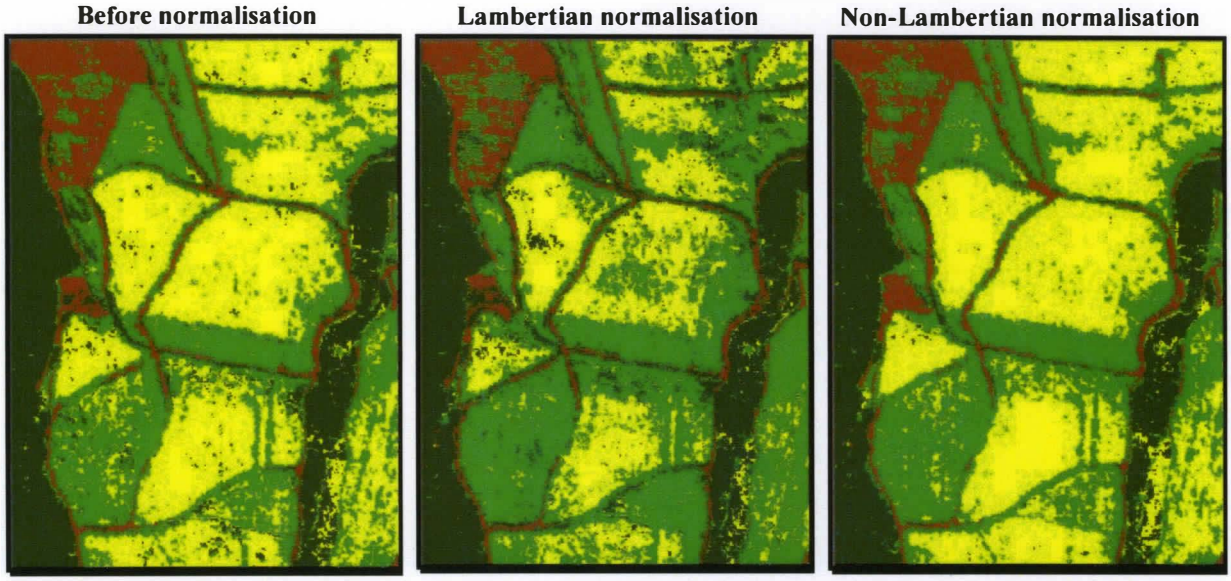

Figure 4.4, result of the three classifications

Color	Class
	Sugar cane variety R70
	Sugar cane variety R74
	Forest
	Bare soil

Table 4.2, legend of the classified image

5.0 Conclusion and recommendations

The normalisation of the CASI image was performed and evaluated for the Lambertian and non-Lambertian models. The normalisation model parameters, derived from the topographic characteristics of the study area, were given by DEM, generated from aerial photography stereoscopic analysis.

The derivation of the topographic parameters is the main step in the image normalisation. The precision of the DEM has to be adequate with the metric resolution of the image, 2 meters in this study. This was the main difficulty in the generation of the DEM using stereoscopic analysis. A recommendation for this step is to use a GPS in differential correction mode. The use of a GPS receiver is more accurate in terms of operator time and precision of the DEM (under the meter).

The validation of the performance of the model was assessed using 3 indicators, visual analysis, statistical analysis and evaluation of the improvement of the classification accuracy. The result shows that neither Lambertian nor non-Lambertian normalisation model has improved the accuracy of the supervised classification. The Lambertian model decreases more the classification accuracy than the non-Lambertian model, this result explains an over correction of both normalisation model.

The statistical analysis based on the comparison of the DN value variation on an homogenous area has shown that neither the Lambertian nor non-Lambertian model has decrease the coefficient of variation. On the contrary, both model increase the variation of the pixels brightness value on an homogenous area.

The diminution of the perception of the forms of the relief was archived only for the Lambertian correction. The problem of over correction is still present.

The result obtained in this study has to be interpreted carefully in relation with the study area topographic characteristics, homogenous aspect and low slope (7%). In this area the topographic effect seems to be insignificant on the radiometry of the CASI image. This is in line with the finding in the evaluation of the performance of the model, over correction by the two models. This could be due to the high metric resolution (2 meters) of the CASI image.

It would be very interesting to pursue this project using a study area with more heterogeneous topographic characteristics in term of slope and aspect variation. The topographic effect on high metric resolution data should be investigated as we will more and more be given images with such metric resolution to work on by the present and future generation of commercial satellites.

Appendix 1 – Compact Airborne Spectrographic Imager

CASI uses a two-dimensional Charge Coupled Device (CCD) array with 288 elements in the spectral direction and 612 pixels in the spatial direction of which 512 pixels are available for imaging. The 288 basic spectral bands have a band centre spacing of 1.9 nm, a bandwidth of 2.2 nm, and together span a range of 545 nm, which is selectable within the 400 nm to 1000 nm range. The signals from each of these bands are digitised to 16 bits.

In the full spectral mode, all 288 basic bands are recorded, but the swath is limited to 39 pixels. In the full spatial mode, the full swath of 512 pixels is recorded for up to 20 preselected spectral bands.

The sensor can also be operated in modes in which intermediate numbers of spectral bands and pixels are recorded. These bands can be formed of sums of up to 16 basic bands; their centre positions and bandwidths are programmable.

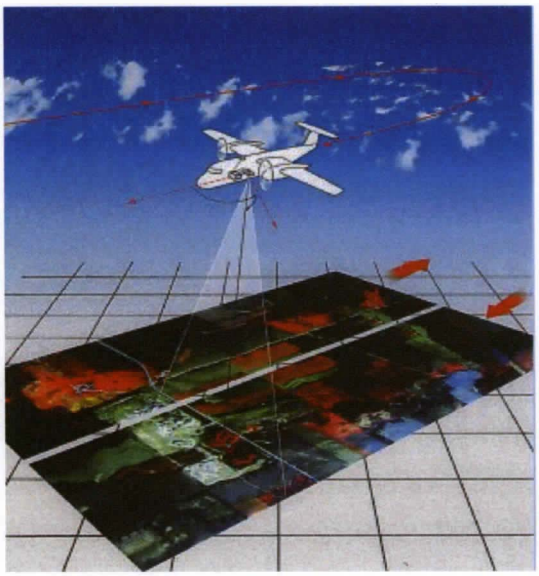

The CASI in flight

The different component of the CASI

Appendix 1a – CASI true color composite

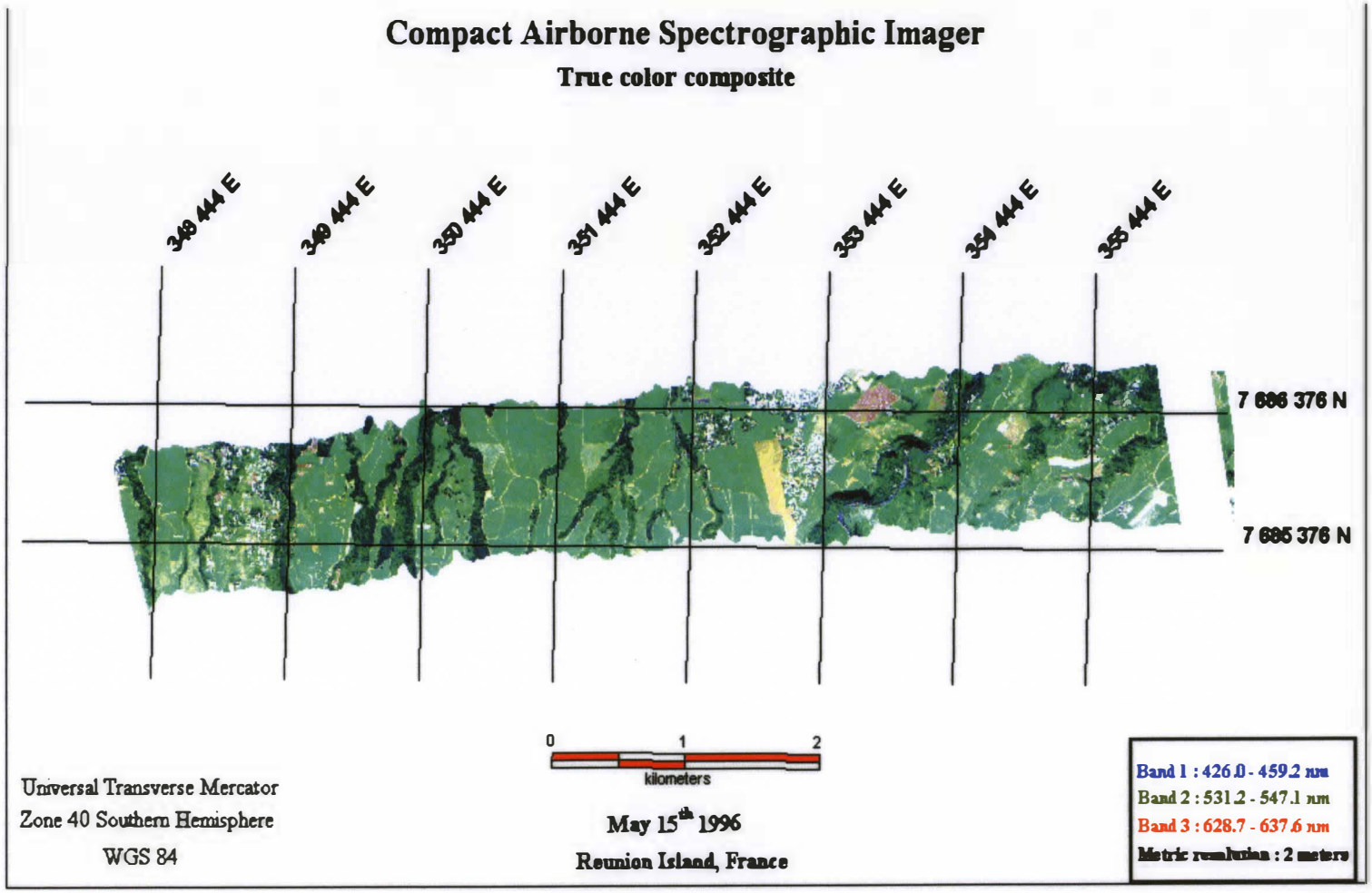

Appendix 2 – Location of the 15 GPS points used for the absolute orientation of the stereoscopic couple

Appendix 3 - DEM Product Generation

The terrain analysis tools in Erdas imagine were used to generate slope and aspect images from the elevation data.

Slope image
The slope is calculated for each pixel using a 3x3 pixel window using equations A1 and A2:

$$S = (((\Delta x)^2+(\Delta y)^2)^{0.5}) / 2 \qquad \textbf{(A1)}$$

Where:
S = fractional slope
Δx = average elevation change in x
Δy = average elevation change in y

$$\theta_n = \tan^{-1}(s) \qquad \textbf{(A2)}$$

Where:
θ_n =Slope in radians

Aspect image
The aspect image is calculated according to the prevailing direction of the slope at each pixel, again using a 3x3-pixel window, using the formula below. Aspect is expressed as degrees clockwise from north. A horizontal surface has no aspect, and is assigned a value of 361 degrees.

$$\phi_n = \pi+\tan^{-1}(\Delta x/\Delta y) \qquad \textbf{(A3)}$$

Where:
ϕ_n = aspect (in radians)

Cos(i) and cos(e) images
From the slope and aspect rasters, the cos(i) and cos(e) images, which act as the inputs to the topographic normalisation models, were generated. The cos(i) image was generated in the spatial modeller, using the formula:

$$\cos(i) = \cos\theta_s\cos\theta_n + \sin\theta_s\sin\theta_n\cos(\phi_s - \phi_n) \quad \textbf{(A4)}$$

Where:

i = incidence angle	θ_n = Surface normal zenith (slope)
e = exitance angle	ϕ_s = Solar azimuth
θ_s = Solar zenith angle	ϕ_n = Surface azimuth (aspect)

Appendix 3a – Triangulated Irregular Network

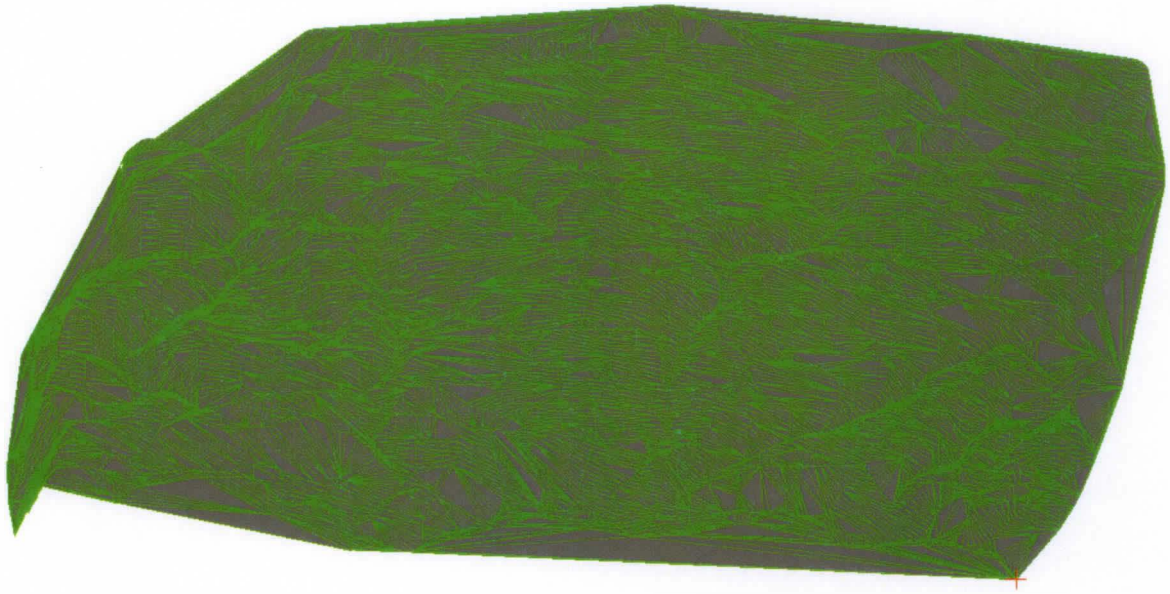

Triangulated Irregular Network representation of the DEM

Appendix 4 – Land use data

Layout of the sugar cane field

N°Polygons	Variety	Plantation date	Stage	Harvesting in 95	Harvesting in 96
1	R570	beginning of 1993	2 growth	04-sept	05-oct
2	R570	beginning of 1993	2 growth	04-sept	05-oct
3	R570	beginning of 1993	2 growth	04-sept	05-oct
4	R574	beginning of 1994	1 growth	28-jul	14-sept
5	R574	beginning of 1992	3 growth	25-sept	18-oct
6	R570	beginning of 1994	1 growth	28-jul	14-sept
7	R574	beginning of 1992	3 growth	25-sept	18-oct
8	R574	beginning of 1992	3 growth	12-oct	26-oct

12	R570	beginning of 1993	2 growth	04-sept	05-nov
13	R570	beginning of 1995	blank		29-jul
14	R570	beginning of 1995	blank		15-febr
15	R574	beginning of 1995	blank		23-august
16	R578	beginning of 1991	4 growth	14-sept	03-oct
25	R570	beginning of 1995	blank		15-nov
26	R570	beginning of 1995	blank		15-nov
29	R574	beginning of 1987	5 growth	30/10/92	12-nov
34	R574	beginning of 1995	blank		31- august
36	R572	beginning of 1993	2 growth	28-sept	16-sept
37	R570	beginning of 1991	4 growth	11-oct	16-nov
38	R574	beginning of 1991	4 growth	10-oct	25-oct
39	R570	beginning of 1995	blank		17-sept
40	R570	beginning of 1991	4 growth	11-oct	16-nov
41	R570	beginning of 1993	2 growth	30- august	15-sept
42	R570	beginning of 1991	4 growth	01-sept	03-oct
1'	R570	beginning of 1991	4 growth	16-oct	22-nov
6'	R570	beginning of 1992	3 growth	25-jul	09- august

Appendix 5 – Detailed results of the classification

CLASSIFICATION ACCURACY ASSESSMENT REPORT
Lambertian model

ERROR MATRIX

Classified Data	cane1	cane2	bare soil	forest	Row Total
cane1	11	6	0	1	18
cane2	3	5	0	1	9
bare soil	1	0	6	0	7
forest	0	1	1	4	6
Column Total	15	12	7	6	40

ACCURACY TOTALS

Class Name	Reference Totals	Classified Totals	Number Correct	Producers Accuracy	Users Accuracy
cane1	15	18	11	73.33%	61.11%
cane2	12	9	5	41.67%	55.56%
bare soil	7	7	6	85.71%	85.71%
forest	6	6	4	66.67%	66.67%
Totals	40	40	26		

Overall Classification Accuracy = 65.00%

KAPPA (K^) STATISTICS

Overall Kappa Statistics = 0.5075

Conditional Kappa for each Category.

ClassName	Kappa
cane1	0.3778
cane2	0.3651
bare soil	0.8268
forest	0.6078

CLASSIFICATION ACCURACY ASSESSMENT REPORT
non-Lambertian model

ERROR MATRIX

Classified Data	Forest	bare soil	cane2	cane1	Row Total
Forest	4	0	0	0	4
bare soil	0	6	0	1	7
cane2	0	0	18	0	18
cane1	1	1	7	2	11
Column Total	5	7	25	3	40

ACCURACY TOTALS

Class Name	Reference Totals	Classified Totals	Number Correct	Producers Accuracy	Users Accuracy
Forest	5	4	4	80.00%	100.00%
bare soil	7	7	6	85.71%	85.71%
cane2	25	18	18	72.00%	100.00%
cane1	3	11	2	66.67%	18.18%
Totals	40	40	30		

Overall Classification Accuracy = 75.00%

KAPPA (K^) STATISTICS

Overall Kappa Statistics = 0.6183

Conditional Kappa for each Category.

Class Name	Kappa
Forest	1.0000
bare soil	0.8268
cane2	1.0000
cane1	0.1155

References

Chavez, P.S., Jr., and W.B., Mitchell, 1977, Computer enhancement techniques of Landsat MSS digital images for land use and land cover assessment, Proceeding of the 6th Annual Remote Sensing of Earth Resources Conference, pp. 259-276.

Colby, J. D., 1991. Topographic Normalization in Rugged Terrain. *Photogramm. Eng. Remote Sens.* 57(5):531-537.

Holben, B. N., and C. O. Justice, 1980. The Topographic Effect on Spectral Response from Nadir-Pointing Sensors. *Photogramm. Eng. Remote Sens.* 46(9):1191-1200.

Holmes, G.J., 1998. Detection and Normalisation of the Topographic Effect in SPOT Imagery of the English Peak District. MSc Thesis, Silsoe College Library.

Jones, A.R., Settle, J.J., et Wyatt, B.K., 1988, Perspective images from the SPOT-1 HRV sensor, Int. J.Remote Sens. 9, 1405-1407.

Kimes, D.S., and J.A. Kirchner, 1981. Modelling the effects of various radiant transfers in mountainous terrain on sensor response, IEEE Transaction on Geoscience and Remote Sensing, 19(2):100-108.

Kowalik, W.S., R.J.P. Lyon, and P. Switzer, 1983. The effects of additive radiance terms on ration of Landsat data, Photogrammetric Engineering & Remote Sensing, 49(5):659-669.

Leprieur, C. E., J. M. Durand, and J. L. Peyron, 1988. Influence of Topography on Forest Reflectance Using Landsat Thematic Mapper and Digital Terrain Data. *Photogramm. Eng. Remote Sens.* 54(4):491-496.

Proy, C., D. Tancré, and P.Y. Deschamps, 1989. Evaluation of topographic effects in remotely sensed data, Remote sensing of environment, 30:21-32.

Reeder, D. et al., 1999, Removing the Topographic Effect from Digital Satellite Data, ERIM 13th International conference on Applied Geologic Remote Sensing, Vancouver, Canada.

Rowan, L.C., A.F.H. Goetz, and R.P. Ashley, 1977. Discrimination of hydrothermally altered and unaltered rocks in visible and near infrared multispectral images, Geophysics, 42(3):522-535.

Smith, J.A., Kin, T.L., et Ramson, K.J., 1980, The lambertian assumption and Landsat data, Photogramm. Eng. Remote Sens. 46, pp.1183-1189.

Teillet et al., 1982, On the slope-aspect correction of multispectral scanner data, Canadian Journal of remote sensing, Vol.8, N°2, december 1982.

Thomson, A.G., and C. Jones, 1990. Effect of topography on radiance from upland vegetation in North Wales, International Journal of Remote Sensing, 11(5):829-840.

Yang, J.Y., 1990. Correction radiométrique des effets topographiques sur les images satellitaires, Thèse de Doctorat, Univ. de Toulouse, France, p.120.